Journal of Chemical Crystallography (2025) 55:56–65
https://doi.org/10.1007/s10870-024-01035-0

ORIGINAL PAPER

Polymorphism and Whole-Molecule Disorder of an Antitubercular 8-Nitrobenzothiazinone

Rüdiger W. Seidel[1] · Richard Goddard[2] · Tom U. Schlegel[1,3] · Adrian Richter[1] · Ines Rudolph[1] · Peter Imming[1]

Received: 4 September 2024 / Accepted: 18 November 2024 / Published online: 7 December 2024

Abstract

8-Nitrobenzo-1,3-thiazin-4-ones (BTZs) are a promising class of antitubercular agents with a novel mechanism of action, viz. suicide inhibition of decaprenylphosphoryl-β-D-ribose 2'-epimerase 1 (DprE1), an enzyme crucial for cell wall synthesis in the pathogen *Mycobacterium tuberculosis*. 8-Nitro-2-(piperidin-1-yl)-6-(trifluoromethyl)-4*H*-benzo-1,3-thiazin-4-one (**1**) is a chemically simplified analogue of the anti-tuberculosis phase 2 clinical drug candidate BTZ-043. Structural elucidation of **1** in the solid-state has been carried out by X-ray crystallography and two polymorphic forms of **1** have been revealed. **1**-I crystallizes in the triclinic system (space group *P*-1, *Z*=6) with one molecule exhibiting whole-molecule disorder with a preferred orientation. The crystal structure of **1**-II belongs to the tetragonal system (space group $P4_3$, *Z*=4) and exhibits positional disorder in several parts of the molecule.

Graphical Abstract

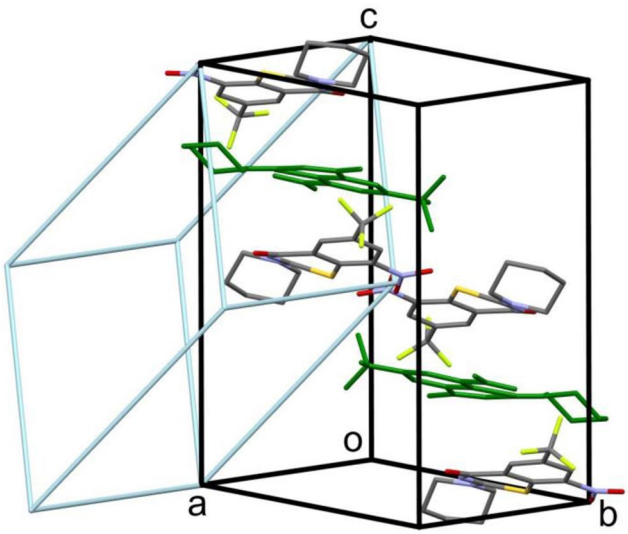

X-ray crystallography revealed a triclinic (space group *P*-1, *Z*=6) and a tetragonal (space group $P4_3$, *Z*=4) polymorph of the antimycobacterial agent 8-nitro-2-(piperidin-1-yl)-6-(trifluoromethyl)-4*H*-benzo-1,3-thiazin-4-one

Keywords Benzothiazinone · Crystal structure · Polymorphism · Disorder · Tuberculosis

✉ Rüdiger W. Seidel
ruediger.seidel@pharmazie.uni-halle.de

[1] Institut für Pharmazie, Martin-Luther-Universität Halle-Wittenberg, Wolfgang-Langenbeck- Str. 4, 06120 Halle (Saale), Germany

[2] Max-Planck-Institut für Kohlenforschung, Kaiser-Wilhelm-Platz 1, 45470 Mülheim an der Ruhr, Germany

[3] Present address: Institut für Wirkstoffentwicklung, Universität Leipzig, Liebigstr. 19, 04103 Leipzig, Germany

Introduction

Tuberculosis (TB) continues to be a global public health issue. TB is a debilitating infectious disease caused by *Mycobacterium tuberculosis* [1], which primarily affects the lungs but can also manifest as extrapulmonary disease [2]. According to the World Health Organization (WHO), an estimated 10.6 million people fell ill with and a total of approximately 1.3 million died of TB in 2022 [3]. Especially drug-resistant TB has become a global health concern and a particular threat in certain regions of the world [4, 5]. In the 2024 Bacterial Priority Pathogens List update, the WHO newly included rifampicin-resistant *M. tuberculosis* in the critical group because of the pathogen's ability to transfer resistance genes, the severity of the disease caused and the significant global burden [6]. This underscores the critical need for new antibiotics with novel mechanisms of action to combat drug-resistant TB [7–13].

8-Nitrobenzo-1,3-thiazin-4-ones (BTZs) have been identified as potent antitubercular agents in a seminal work by Makarov et al. [14]. BTZs block the mycobacterial cell wall synthesis through covalently binding to the enzyme decaprenylphosphoryl-β-D-ribose 2'-epimerase 1 (DprE1) [15] after reduction to the 8-nitroso form (mechanism-based inhibition) [16]. An up-to-date perspective on this compound class has been published recently [17]. The most advanced candidate, namely BTZ-043 (Fig. 1), is presently being investigated in phase 2 clinical studies [18]. Compound **1** (Fig. 1) represents a chemically simplified analogue of BTZ-043, in which the (*S*)-2-methyl-1,4-dioxa-8-azaspiro[4.5]decan-8-yl side chain appended to position 2 of the BTZ scaffold is replaced by a piperidinyl group. The lack of the spiroketal moiety, however, reduces the in vitro activity against *M. tuberculosis* and other mycobacteria. Nonetheless, **1** remains a potent antimycobacterial agent with a minimum inhibitory concentration against *M. tuberculosis* at the micromolar level [19–23].

As far as we are able to ascertain, compound **1** was reported for the first time by Gao et al. in 2013, in the course of a structure-activity-relationships (SAR) study on antitubercular BTZs [21]. In a recent perspective, we reviewed various methods for the synthesis of **1** [17]. Apart from the synthesis and antimycobacterial evaluation, we also investigated the chemical reactivity of **1** towards oxidizing [24] and reducing agents [19, 22], in addition to the Grignard reagent methylmagnesium bromide [19]. Recently, we structurally characterized the azoxy derivative of **1** [25]. To the best of our knowledge and based on a search of the Cambridge Structural Datase (CSD) [26], the crystal and molecular structure of **1** has not been unveiled so far. Here we report the structural elucidation of **1** by X-crystallography, which has so far proved elusive.

Experimental

Synthesis and Crystallization

Compound **1** was synthesized following one of the previously reported procedures [20]. An ATR-FT-IR spectrum of **1** as synthesized can be found in the supplementary material. Crystals of **1**-I suitable for single-crystal diffraction were obtained by diffusing heptane into a solution of **1** in chloroform and those of **1**-II by diffusing hexane into a solution of **1** in ethanol.

X-Ray Crystallography

The diffraction data were measured on a Bruker AXS Kappa diffractometer equipped with an Apex II detector for **1**-I, and on a Bruker AXS D8 Venture diffractometer with a Photon III detector for **1**-II. Mo K_α radiation from an Incoatec IμS microfocus X-ray source with Montel multilayer optics was used in both cases. The APEX5 software

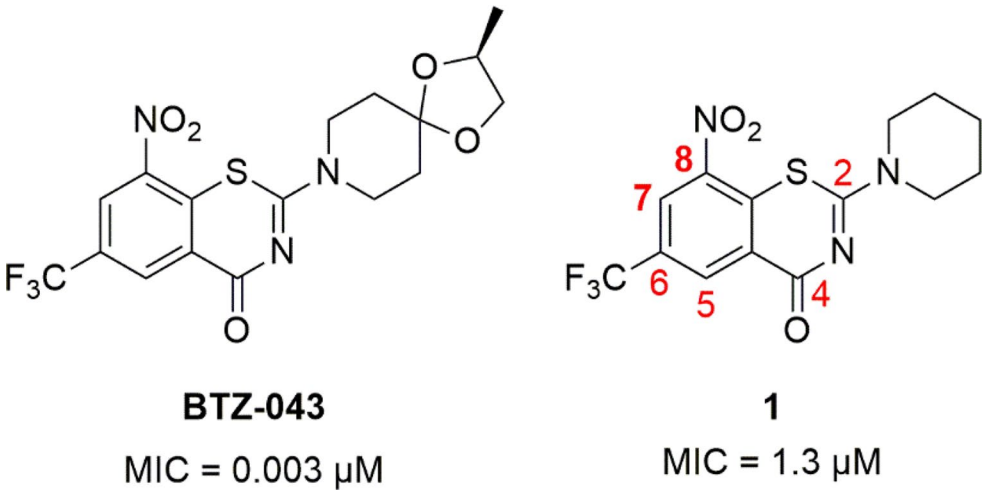

Fig. 1 Chemical diagrams of the antitubercular benzothiazinones BTZ-043 and **1** (with systematic numbering of the BTZ scaffold) and their minimum inhibitory concentrations (MICs) against *M. tuberculosis* H37Rv [20]

[27] was used to control the data collections, and the diffraction data were processed with SAINT [28]. Absorption corrections based on the Gaussian method were carried out with SADABS [29]. The crystal structures were solved with SHELXT [30] and refined with SHELXL [31]. Anisotropic atomic displacement parameters (ADPs) were introduced for all non-hydrogen atoms, except for the minor part of the fully disordered molecule in **1**-I. Disordered parts in **1**-I and **1**-II were modelled with the aid of appropriate geometric restraints as well as restraints or constraints on ADPs (see supplementary crystallographic data). Hydrogen atoms were placed in geometrically calculated positions and refined using the appropriate riding model. The absolute structure of **1**-II was established from anomalous dispersion using Parsons' quotient method [32], resulting in a Flack *x* parameter of 0.02(2). Structure pictures were drawn with Diamond [33] and Mercury [34]. Table 1 lists crystal data and refinement details for **1**-I and **1**-II.

Computational Methods

Density functional theory (DFT) calculations on the free molecule of **1** were performed starting from the molecular structure of unique molecule 1 in the crystal structure of **1**-I using ORCA 6.0 [35] with a B3LYP/G (VWN1) hybrid functional [36, 37] (20% HF exchange) and a def2-TZVPP basis set [38] with an auxiliary def2/J basis [39]. Optimization of the structure used the BFGS method from an initial Hessian according to Almlöf's model with a very tight self-consistent field convergence threshold [40]. The optimized local minimum-energy structures exhibited only positive modes. The calculated IR spectrum was scaled by 0.96 (empirical fit) [41]. Structure pictures were drawn with Diamond [33] and Mercury [34]. Cartesian coordinates of the DFT-calculated molecular structure of **1** can be found in the Supporting Information.

Results

Crystal Structure of 1-I

The triclinic form **1**-I crystallizes in the centrosymmetric space group *P*-1 with the asymmetric unit comprising three molecules (*Z'* = 3). Several crystal specimens were investigated by single-crystal X-ray diffraction at different temperatures. The best diffraction dataset was acquired at 200 K, but we note that no phase change was observed upon cooling to 100 K. The diffraction images show the presence of alternating strong and weak reflections (Fig. 2).

Figure 3a shows the asymmetric unit of **1**-I, and Fig. 2b-d shows the molecular structures of the corresponding three crystallographically unique molecules (labelled 1–3). Molecule 2 exhibits whole-molecule disorder over two positions. The ratio of occupancies refined to 0.832(3):0.168(3). The benzothiazinone scaffolds in molecules 1–3 show some

Table 1 Crystal data and refinement details for **1**-I and **1**-II

	1-I	**1**-II
Empirical formula	$C_{14}H_{12}F_3N_3O_3S$	$C_{14}H_{12}F_3N_3O_3S$
M_r	359.33	359.33
T (K)	200(2)	100(2)
Crystal system, space group	Triclinic, *P*-1	Tetragonal, $P4_3$
a (Å)	11.4394(5)	10.3270(4)
b (Å)	11.4703(5)	10.3270(4)
c (Å)	17.3113(7)	13.8596(8)
α (°)	87.411(2)	90
β (°)	81.367(2)	90
γ (°)	84.321(2)	90
V (Å^3)	2233.65(17)	1478.08(14)
Z, ρ_{calc} (g cm^{-3})	6, 1.603	4, 1.615
μ (mm^{-1})	0.272	0.274
F(000)	1104	736
Crystal size (mm)	0.087 × 0.047 × 0.026	0.220 × 0.081 × 0.043
θ range (°)	1.190–28.375	2.460–30.536
Reflections collected / unique	62,482 / 11,144	173,431 / 4384
R_{int}	0.0637	0.0615
Observed reflections [$I>2\sigma(I)$]	5925	3920
Data / restraints / parameters	11,144 / 446 / 756	4384 / 278 / 292
Goodness-of-fit on F^2	1.011	1.091
R_1 [$I>2\sigma(I)$]	0.0759	0.0481
wR_2 (all data)	0.2298	0.1188
$\Delta\rho_{max}$, $\Delta\rho_{min}$ (eÅ^{-3})	0.455 / −0.419	0.319, −0.374

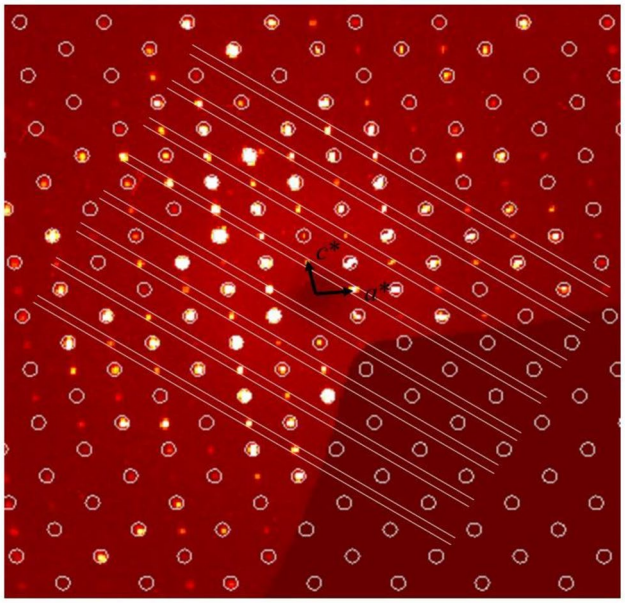

Fig. 2 Reconstruction of the (*h*0*l*) reciprocal space layer for the supercell of **1**-I from one $\phi\varphi$ scan, showing the alternating weak and strong reflections. Weak reflections (*hkl*: $h+k+l=2n+1$) are highlighted for eight reciprocal lattice planes by double lines. Circles represent calculated positions of reflections in the small unit cell obtained by ignoring the weak reflections (see Section "Discussion")

deviation from planarity. A slight boat shape of the thiazinone moiety is most apparent in molecules 1 and 3. The $-CF_3$ group in molecule 3 exhibits rotational disorder over two positions with a ratio of occupancies of 0.593(5):0.407(5). The piperidinyl ring adopts a chair conformation in each case.

Figure 4 illustrates the crystal packing of **1**-I. As shown in Fig. 3a, unique molecules 1 and 3 form antiparallel centrosymmetric stacks each with a symmetry-related molecule about a centre of symmetry. Unique molecule 2 is rotated by approximately 90° and sandwiched in between these stacks with whole-molecule disorder (not shown in Fig. 3a; cf. Fig. 3c). Figure 4b depicts the resulting columnar arrangement of the molecules along the [11-1] direction.

Crystal Structure of 1-II

The tetragonal crystal form **1**-II crystallizes in the chiral space group $P4_3$ with four molecules in the unit cell ($Z=4$). Figure 5 depicts a displacement ellipsoid plot of the molecular structure of **1** in the crystal of **1**-II. The thiazine moiety with the tethered piperidinyl group, the $-CF_3$ and the $-NO_2$ group were each found to be disordered over two positions. The ratio of occupancies refined to 0.724(6):0.276(6), 0.852(6):0.148(6) and 0.634(8):0.366(8), respectively. The chair conformation is observed for the piperidinyl ring.

In the crystal, the molecules stack along a 4_3 screw axis (left-handed) parallel to the crystallographic *c* axis direction, passing approximately through the centres of the thiazine six-membered rings (Fig. 6a). Thus, adjacent molecules within a stack are rotated by 90°. Figure 6b depicts the crystal packing of **1**-II, revealing the columnar arrangement of the stacks parallel to the *c* axis direction. There are no unexpectedly short intermolecular contacts in the structure.

Density Functional Theory (DFT) Study of 1

The structure of the free molecule of **1** was optimized by DFT calculations. Figure 7 depicts the resulting calculated molecular structure. The benzothiazinone scaffold is not entirely planar, but the thiazinone moiety is slightly boat-shaped. The angle between the mean plane through S1, C2, N3 and C4 and the mean plane through the benzene ring is 7.6°. The plane of the nitro group is tilted out of the latter plane by 6.9°. The S1···O2 distance is 2.60 Å and the C8A−S1···O2 angle is 177.2°. The coordination at N2 is virtually planar and the piperidinyl ring adopts a chair conformation with minor angular deviations from the ideal tetrahedral value.

Discussion

Structural insight and an understanding of solid-state characteristics, such as the existence of polymorphic crystal forms, of pharmaceutically relevant compounds is important for their successful development [42]. Polymorphs I and II of the antitubercular BTZ **1** crystallized at room temperature from different solvent systems. Solvent-dependence of polymorphic crystallization is well known [43]. X-ray crystallography revealed the crystal structures of forms **1**-I and **1**-II.

The diffraction data for the triclinic **1**-I were indexed in the superstructure ($V=2234$ Å^3) with $Z=6$, which is based on both main and weak reflections (Fig. 2). This led to the refinement model described above, with three symmetry-independent molecules ($Z' = 3$) in the space group *P*-1 and with occupational modulation [44] of the fully disordered unique molecule 2 (Fig. 3). Ignoring the weak reflections, a triclinic unit cell with half of the volume of the supercell ($V=1117$ Å^3) and $Z=3$ results. Accordingly, the asymmetric unit then contains two molecules, of which one is disordered about a centre of symmetry and thus has a site occupancy factor of 0.5 for each orientation (resulting in Z' = 1.5). Although this model also refined well, we chose the superstructure taking the weak reflections into account for the final refinement. In the small unit cell, the ratio of occupancies of the molecule disordered about an inversion centre

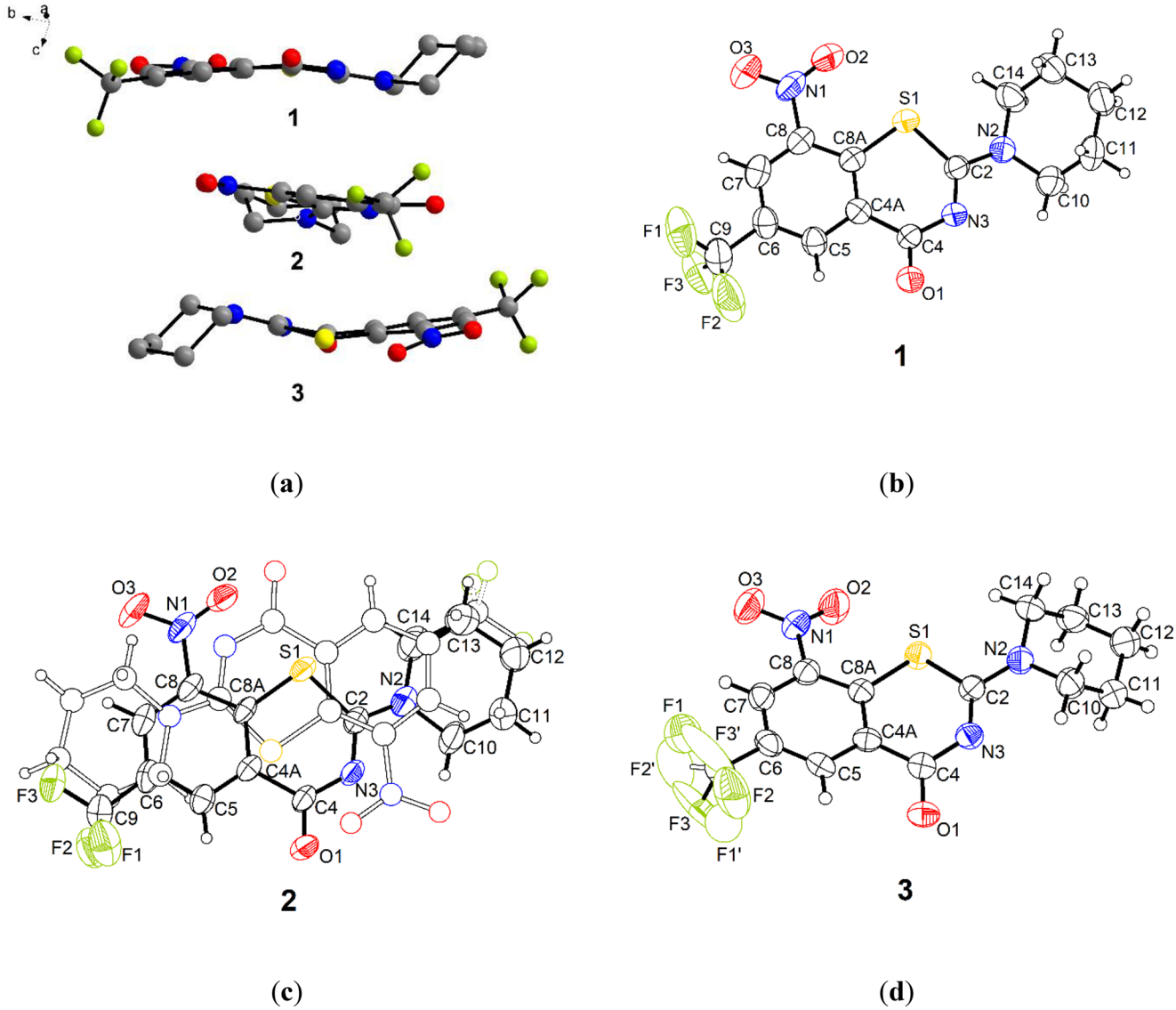

Fig. 3 (**a**) Asymmetric unit of **1**-I. Disorder and H atoms are not shown for clarity. Colour scheme: **C**, grey; F, lime; N, blue; O, red; S, yellow. (**b**)-(**d**) Molecular structures of the crystallographically unique molecules 1–3 (cf. part **a**). Displacement ellipsoids are drawn at the 50% probability level. The minor part of the whole-molecule disorder of molecule 2 (17% occupancy) is shown as empty ball-and-stick model, and the minor part of the disordered $-CF_3$ group in molecule 3 (41% occupancy) with empty ellipsoids. H atoms are shown as small spheres of arbitrary radius

is 0.5:0.5 by virtue of symmetry, which is actually the average of 0.832(3):0.168(3) and 0.168(3):0.832(3), as found respectively for the fully disordered unique molecule 2 and its symmetry-related molecule in the supercell (Fig. 8). The occupational modulation of molecule 2 would go unnoticed if the weak reflections were ignored. The crystal structure of **1**-I thus represents a case of pseudosymmetry, which describes a spatial arrangement that mimics a higher crystallographic symmetry without fulfilling it exactly [45, 46]. Specifically, in **1**-I we have *pseudo I*-centring of the crystal lattice, meaning that a non-crystallographic symmetry operator generates a translational pseudosymmetry operator that is very similar to a crystallographic *I*-centring operator. In reciprocal space, this situation leads to a systematic modulation of the observed intensities with the reflections that would be systematically absent for exact *I*-centring having systematically low intensities (Fig. 2) [47].

For the tetragonal crystal form **1**-II, the absolute structure, i.e. the handedness of the fourfold screw axis (chiral space group $P4_3$), was unequivocally determined by the analysis of anomalous scattering effects, resulting in a Flack *x* parameter close to zero with a small standard uncertainty (Section "X-ray crystallography") [48].

The crystal structure determinations of **1**-I and **1**-II unambiguously confirmed the molecular structure of **1**. Detailed discussion of molecular geometry parameters in the

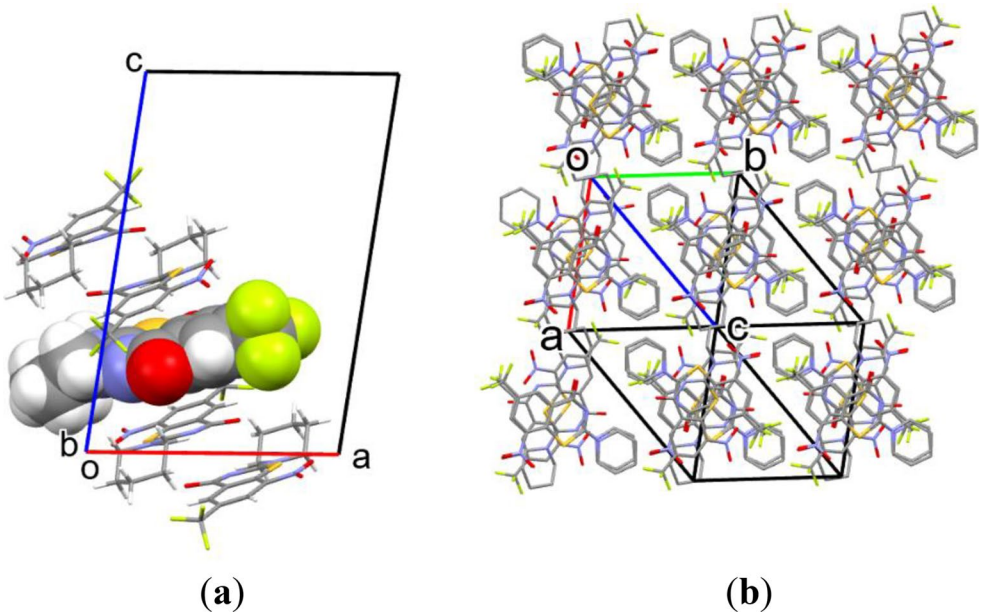

Fig. 4 (**a**) Part of the crystal structure of **1**-I, viewed along the *b* axis direction. Unique molecule 2 is shown in space-filling representation. (**b**) Packing diagram of **1**-I, viewed along the [11-1] direction (H atoms omitted clarity). Disorder is not shown for the sake of clarity. Colour scheme: C, grey; H, white; F, lime; N, blue; O, red; S, yellow

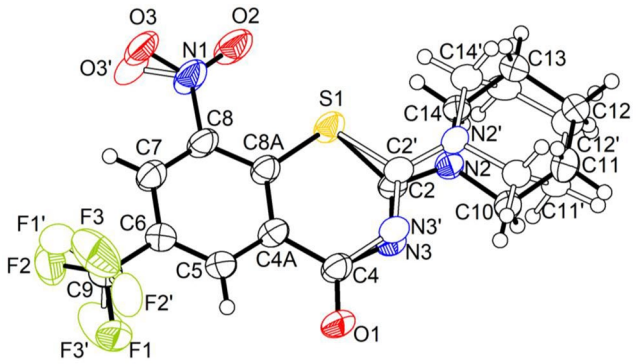

Fig. 5 Molecular structure of **1** in the crystal of **1**-II. Displacement ellipsoids are drawn at the 50% probability level. Small spheres of arbitrary radius represent H atoms. Disorder parts with minor occupancies are shown with empty ellipsoids

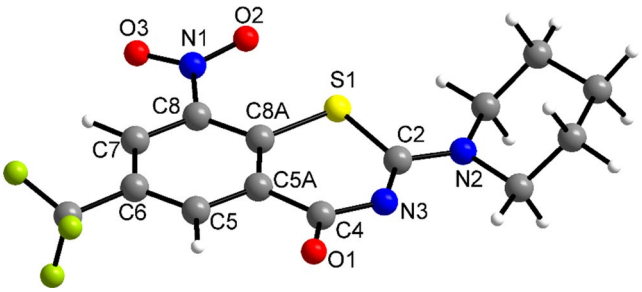

Fig. 7 DFT-calculated molecular structure of the isolated molecule of **1**. Colour scheme: C, grey; H, white; F, lime; N, blue; O, red; S, yellow

solid-state structures of **1**-I and **1**-II is hampered by disorder. Merely unique molecule 1 in **1**-I was found completely unaffected by disorder (Fig. 3b). Nonetheless, in Fig. 3a it

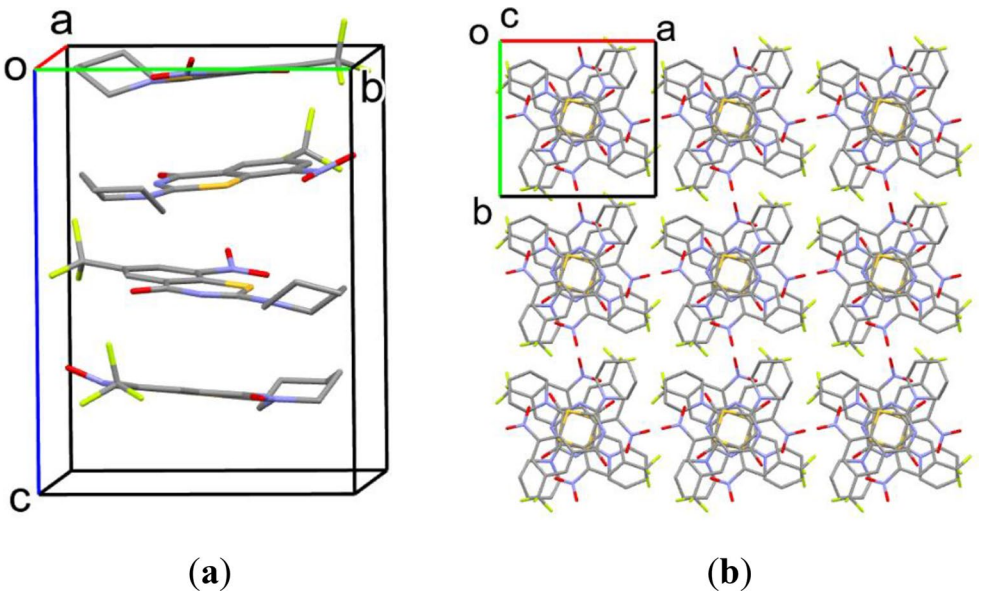

Fig. 6 (**a**) Tetragonal unit cell of **1**-II, projected approximately along the *a* axis direction. (**b**) Packing diagram of **1**-I, viewed along the *c* axis direction. H atoms and disorder parts with minor occupancies are not shown for clarity. Colour scheme: C, grey; F, lime; N, blue; O, red; S, yellow

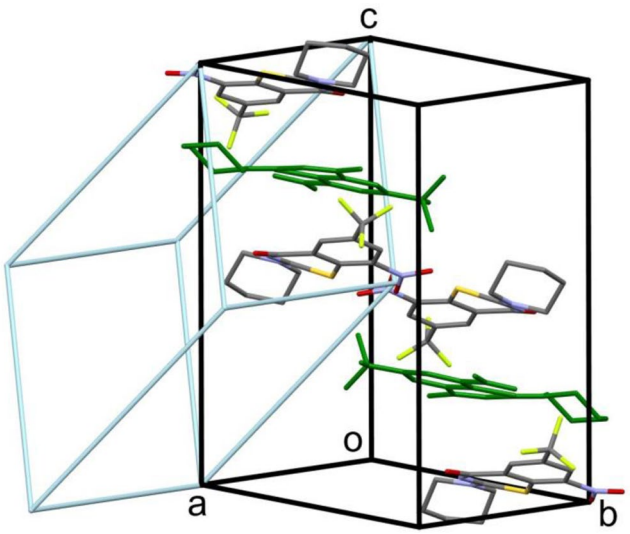

Fig. 8 Relationship between the small unit cell of **1**-I (light blue) and the *pseudo I*-centred supercell. Fully disordered molecules are shown in dark green for the major component, illustrating the different orientations of the major components in the two halves of the supercell. Hydrogen atoms omitted for clarity. Colour scheme: C, grey; F, lime; N, blue; O, red; S, yellow

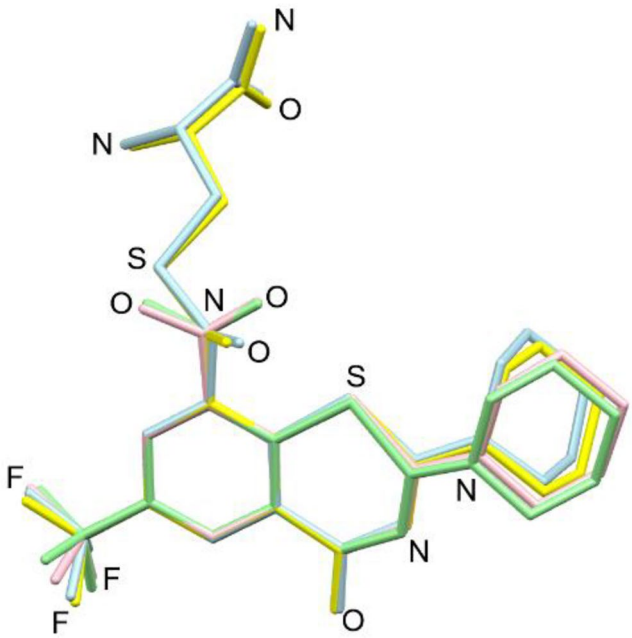

Fig. 9 Structure overlay plot of molecule 1 in **1**–1 (green), the DFT-optimized structure of the free molecule (pink) and the two crystallographically independent ligands covalently bound to Cys387 of *M. tuberculosis* DprE1 (light blue and yellow; PDB refcode: 6HFV) [22]. The structures are superimposed at the benzene rings. Heteroatoms are labelled for easy orientation, and hydrogen atoms are omitted for clarity

can be seen that the BTZ scaffolds are distinctly non-planar in unique molecules 1 and 3 in **1**-I. To gain insight into the structure of the free molecule of **1** and to reveal possible effects of crystal packing on the molecular structure, we performed DFT calculations. In the DFT-optimized structure (Fig. 7), a slight boat-shape of the thiazinone moiety is also noticeable, albeit to a lesser extent than in unique molecules 1 and 3 in **1**-I. The angle between the mean plane through S1, C2, N3 and C4 and the mean plane through the benzene ring is 7.6° for the free calculated molecule, 14.2° for molecule 1 and 22.9° for molecule 3. This suggests that the observed deviation from planarity is not exclusively due to packing effects in the solid-state. The intramolecular short contact between the nitro oxygen atom O2 and the BTZ sulfur atom and the C2−S1···O2 angle close to linearity are present in the solid-state and in the DFT-optimized structure of the free molecule. Possibly intramolecular chalcogen bonding along the extension of the C2−S1 bond helps stabilize the structure [49, 50]. In general, sulfur is a scant chalcogen bond donor but bonded electron-withdrawing moieties can increase its electrophilicity. In a recent perspective article [17], we reviewed crystal structures of BTZs published in the CSD [26]. The BTZ thiazinone moiety exhibits some conformational flexibility. There appears to be no obvious simple relationship between a planar or boat-shaped conformation and the substitution pattern on the fused benzene ring or the nature of the side chain appended to C2. In the case of 8-nitro-6-(trifluoromethyl)-BTZs, it is interesting to note that the thiazinone moiety is markedly boat-shaped in the crystal structure of BTZ-043 (Fig. 1; CSD refcode: HACQOV) [51], whereas the BTZ system is nearly planar for example in the structure of *N*-Boc-8-nitro-2-(piperazin-1-yl)-6-(trifluoromethyl)-BTZ (MESSOW) [20].

Figure 9 compares the molecular structures of the non-disordered molecule in **1**-I and the DFT-optimized structure with those of the two crystallographically unique ligands in the protein crystal structure of **1** in complex with *M. tuberculosis* DprE1 (PDB code: 6HFV), albeit obtained by incubation of the enzyme with the 8-hydroxylamine derivative of **1** [22]. Therein, **1** forms a semimercaptal adduct with the thiol group of a cysteine residue (Cys387). Bearing the resolution of the protein crystal structure in mind (d=2.05 Å), the comparison also reveals that the region of the piperidinyl side chain tethered to C2 of the BTZ scaffold is rather flexible. This group, which is located at the protein surface in the complex with DprE1, has also been by far the focus of the most SAR studies of BTZs. The MICs for BTZ-043 and **1** (Fig. 1) demonstrate that the nature of this group has a remarkable impact on the in vitro antimycobacterial activity, but a comprehensive understanding of the phenomenon has not yet been achieved [17].

The crystal packing in polymorphs **1**-I and **1**-II is distinctly different but nonetheless shares some similarities. Both forms feature a columnar arrangement of the molecules (Figs. 4b and 6b). In **1**-I, adjacent molecules within a columnar stack are rotated by 180° (about inversion centres)

and approximately 90° degree in an alternating fashion (Fig. 4a). Antiparallel (*pseudo*) centrosymmetric stacks of BTZs have frequently been encountered in the solid-state [17]. In **1**-II, the molecules stack in a helical fashion along a 4_3 screw axis with neighbouring molecules rotated counter-clockwise by 90°. Presumably, packing problems cause the disorder in both **1**-I and **1**-II and also led to crystallization with $Z' > 1$ in the case of **1**-I [52]. Important directional intermolecular interactions between adjacent columns of molecules are absent in the case of **1**-II. It is worth noting, however, that there are short contacts (H···H ca. 1.67 Å) between major and minor components of the disordered molecules along the *a* axis direction in **1**-I, indicating that the disordered molecules are aligned in neighbouring columns, in which case the short contacts disappear.

Conclusions

We have determined the solid-state structure of the antitubercular BTZ **1** by X-ray crystallography and thereby discovered two polymorphic crystal forms, namely triclinic **1**-I and tetragonal **1**-II. In both forms, columnar stacking of the molecules in the direction approximately perpendicular to the molecular plane is observed. Adjacent molecules within a columnar stack are rotated by 180° and approximately 90° in an alternating fashion in **1**-I and by 90° along a 4_3 screw axis in **1**-II. The asymmetric unit of **1**-I contains three molecules (Z' = 3) with one fully disordered, albeit preferentially oriented. The single crystallographically unique molecule in **1**-II is affected by localized disorder.

Supplementary Information The online version contains supplementary material available at https://doi.org/10.1007/s10870-024-01035-0.

Acknowledgements We would like to thank Professor Christian W. Lehmann for providing access to the X-ray diffraction facility and Heike Schucht and Lucas Schulte-Zweckel for technical assistance with the X-ray intensity data collections.

Author Contributions Conceptualization, R.W.S. and R.G.; methodology, R.W.S. and R.G.; validation, R.W.S. and R.G.; formal analysis, R.W.S. and R.G.; investigation, R.G. and T.U.S.; resources, R.G., A.R. and P.I.; data curation, R.W.S. and R.G.; writing—original draft preparation, R.W.S.; writing—review and editing, R.G., T.U.S., A.R., I.R. and P.I.; visualization, R.W.S. and R.G.; supervision, A.R. and P.I.; project administration, R.W.S.

Data Availability CCDC 2381916 (**1**-I) and CCDC 2381917 (**1**-II) contain the supplementary crystallographic data for this paper. The data can be obtained free of charge from the Cambridge Crystallographic Data Centre via www.ccdc.cam.ac.uk/structures. The corresponding raw data (diffraction images) in the Bruker AXS format can be downloaded from the Edmond research data repository via http://dx.doi.org/10.17617/3.BLYNGQ for **1**-I and http://dx.doi.org/10.17617/3.8WOFVW for **1**-II.

Declarations

Competing Interests The authors declare no competing interests.

References

1. Orgeur M, Sous C, Madacki J, Brosch R (2024) Evolution and emergence of Mycobacterium tuberculosis. FEMS Microbiol Rev 48(2):fuae006. https://doi.org/10.1093/femsre/fuae006
2. Sharma A, De Rosa M, Singla N, Singh G, Barnwal RP, Pandey A, Tuberculosis (2021) An overview of the immunogenic response, Disease Progression, and Medicinal Chemistry efforts in the last decade toward the development of potential drugs for extensively drug-resistant tuberculosis strains. J Med Chem 64:4359–4395. https://doi.org/10.1021/acs.jmedchem.0c01833
3. Global Tuberculosis Report (2023) Geneva, Switzerland: World Health Organization; 2023
4. Farhat M, Cox H, Ghanem M, Denkinger CM, Rodrigues C, Abd El Aziz MS et al (2024) Drug-resistant tuberculosis: a persistent global health concern. Nat Rev Microbiol. https://doi.org/10.1038/s41579-024-01025-1
5. Dheda K, Mirzayev F, Cirillo DM, Udwadia Z, Dooley KE, Chang KC et al (2024) Multidrug-resistant tuberculosis. Nat Rev Dis Primers 10(1):22. https://doi.org/10.1038/s41572-024-00504-2
6. WHO Bacterial Priority Pathogens List (2024) : bacterial pathogens of public health importance to guide research, development and strategies to prevent and control antimicrobial resistance. Geneva: World Health Organization; 2024
7. Butler MS, Vollmer W, Goodall ECA, Capon RJ, Henderson IR, Blaskovich MAT (2024) A review of Antibacterial candidates with New modes of Action. ACS Infect Dis. https://doi.org/10.1021/acsinfecdis.4c00218
8. Dartois V, Dick T (2024) Therapeutic developments for tuberculosis and nontuberculous mycobacterial lung disease. Nat Rev Drug Discovery 23:381–403. https://doi.org/10.1038/s41573-024-00897-5
9. Sachan RSK, Mistry V, Dholaria M, Rana A, Devgon I, Ali I et al (2023) Overcoming Mycobacterium tuberculosis Drug Resistance: Novel medications and repositioning strategies. ACS Omega 8(36):32244–32257. https://doi.org/10.1021/acsomega.3c02563
10. Chauhan A, Kumar M, Kumar A, Kanchan K (2021) Comprehensive review on mechanism of action, resistance and evolution of antimycobacterial drugs. Life Sci 274:119301. https://doi.org/10.1016/j.lfs.2021.119301

11. Fernandes GFS, Thompson AM, Castagnolo D, Denny WA, Dos Santos JL (2022) Tuberculosis drug Discovery: challenges and New Horizons. J Med Chem 65(11):7489–7531. https://doi.org/10.1021/acs.jmedchem.2c00227
12. Shetye GS, Franzblau SG, Cho S (2020) New Tuberculosis drug targets, their inhibitors, and potential therapeutic impact. Transl Res 220:68–97. https://doi.org/10.1016/j.trsl.2020.03.007
13. Wei X, Yue L, Zhao B, Jiang N, Lei H, Zhai X (2024) Recent advances and challenges of revolutionizing drug-resistant tuberculosis treatment. Eur J Med Chem 277:116785. https://doi.org/10.1016/j.ejmech.2024.116785
14. Makarov V, Manina G, Mikusova K, Möllmann U, Ryabova O, Saint-Joanis B et al (2009) Benzothiazinones kill *Mycobacterium tuberculosis* by blocking Arabinan Synthesis. Science 324(5928):801–804. https://doi.org/10.1126/science.1171583
15. Yadav MR, Murumkar PR, Ghuge RB, Barot RR, Chauhan M (2023) Exploring Decaprenylphosphoryl-β-d-Ribose 2′-Epimerase 1 (DprE1): a target for anti-tubercular drugs. Tuberculosis Integr Sci, p. 499–539
16. Trefzer C, Škovierová H, Buroni S, Bobovská A, Nenci S, Molteni E et al (2012) Benzothiazinones are suicide inhibitors of mycobacterial Decaprenylphosphoryl-β-d-ribofuranose 2′-Oxidase DprE1. J Am Chem Soc 134(2):912–915. https://doi.org/10.1021/ja211042r
17. Seidel RW, Richter A, Goddard R, Imming P (2023) Synthesis, structures, reactivity and medicinal chemistry of antitubercular benzothiazinones. Chem Commun (Camb) 59(32):4697–4715. https://doi.org/10.1039/d3cc00356f
18. (2023) Antibacterial agents in clinical and preclinical development: an overview and analysis. Geneva: World Health Organization; 2024
19. Richter A, Seidel RW, Graf J, Goddard R, Lehmann C, Schlegel T et al (2022) New insight into Dearomatization and decarbonylation of antitubercular 4H-Benzo[e][1,3]thiazinones: stable 5H- and 7H-Benzo[e][1,3]thiazines. ChemMedChem 17:e202200021. https://doi.org/10.1002/cmdc.202200021
20. Richter A, Narula G, Rudolph I, Seidel RW, Wagner C, Av-Gay Y et al (2022) Efficient synthesis of Benzothiazinone Analogues with activity against Intracellular Mycobacterium tuberculosis. ChemMedChem 17(6):e202100733. https://doi.org/10.1002/cmdc.202100733
21. Gao C, Ye T-H, Wang N-Y, Zeng X-X, Zhang L-D, Xiong Y et al (2013) Synthesis and structure–activity relationships evaluation of benzothiazinone derivatives as potential anti-tubercular agents. Bioorg Med Chem Lett 23(17):4919–4922. https://doi.org/10.1016/j.bmcl.2013.06.069
22. Richter A, Rudolph I, Möllmann U, Voigt K, Chung C-w, Singh OMP et al (2018) Novel insight into the reaction of nitro, nitroso and hydroxylamino benzothiazinones and of benzoxacinones with Mycobacterium tuberculosis DprE1. Sci Rep 8(1):13473. https://doi.org/10.1038/s41598-018-31316-6
23. Richter A, Seidel RW, Goddard R, Eckhardt T, Lehmann C, Dörner J et al (2022) BTZ-Derived benzisothiazolinones with in Vitro Activity against Mycobacterium tuberculosis. ACS Med Chem Lett 13(8):1302–1310. https://doi.org/10.1021/acsmedchemlett.2c00215
24. Eckhardt T, Goddard R, Lehmann C, Richter A, Sahile HA, Liu R et al (2020) Crystallographic evidence for unintended benzisothiazolinone 1-oxide formation from benzothiazinones through oxidation. Acta Crystallogr C 76(9):907–913. https://doi.org/10.1107/S2053229620010931
25. Richter A, Goddard R, Imming P, Seidel RW (2022) Structural characterization of the azoxy derivative of an antitubercular 8-nitro-1,3-benzothiazin-4-one. Acta Crystallogr E 78(12):1244–1248. https://doi.org/10.1107/S2056989022010842
26. Groom CR, Bruno IJ, Lightfoot MP, Ward SC (2016) The Cambridge Structural Database. Acta Crystallogr B 72:171–179. https://doi.org/10.1107/S2052520616003954
27. APEX5, Madison (2023) Wisconsin, USA: Bruker AXS Inc
28. SAINT V8.40B, Madison (2019) Wisconsin, USA: Bruker AXS Inc.
29. Krause L, Herbst-Irmer R, Sheldrick GM, Stalke D (2015) Comparison of silver and molybdenum microfocus X-ray sources for single-crystal structure determination. J Appl Crystallogr 48(1):3–10. https://doi.org/10.1107/S1600576714022985
30. Sheldrick GM (2015) SHELXT - integrated space-group and crystal-structure determination. Acta Crystallogr A 71:3–8. https://doi.org/10.1107/S2053273314026370
31. Sheldrick GM (2015) Crystal structure refinement with SHELXL. Acta Crystallogr C 71:3–8. https://doi.org/10.1107/S2053229614024218
32. Parsons S, Flack HD, Wagner T (2013) Use of intensity quotients and differences in absolute structure refinement. Acta Crystallogr B Struct Sci Cryst Eng Mater 69(Pt 3):249–259. https://doi.org/10.1107/S2052519213010014
33. Brandenburg K (2018) Diamond. 3.2k4 ed. Crystal Impact GbR, Bonn, Germany
34. Macrae CF, Sovago I, Cottrell SJ, Galek PTA, McCabe P, Pidcock E et al (2020) Mercury 4.0: from visualization to analysis, design and prediction. J Appl Crystallogr 53:226–235. https://doi.org/10.1107/S1600576719014092
35. Neese F (2024) A perspective on the future of quantum chemical software: the example of the ORCA program package. Faraday Discuss. https://doi.org/10.1039/D4FD00056K
36. Becke AD (1993) Density-functional thermochemistry. III. The role of exact exchange. J Chem Phys 98:5648–5652. https://doi.org/10.1063/1.464913
37. Lee C, Yang W, Parr RG (1988) Development of the Colle-Salvetti correlation-energy formula into a functional of the electron density. Phys Rev B 37:785–789. https://doi.org/10.1103/PhysRevB.37.785
38. Weigend F, Ahlrichs R (2005) Balanced basis sets of split valence, triple zeta valence and quadruple zeta valence quality for H to rn: design and assessment of accuracy. Phys Chem Chem Phys 7:3297–3305. https://doi.org/10.1039/B508541A
39. Weigend F (2006) Accurate coulomb-fitting basis sets for H to Rn. Phys Chem Chem Phys 8(9):1057–1065. https://doi.org/10.1039/B515623H
40. Fletcher R (2000) Practical Methods of Optimization, 2nd Edition. 2nd ed. John Wiley & Sons
41. Scott AP, Radom L (1996) Harmonic vibrational frequencies: an evaluation of Hartree–Fock, Møller–Plesset, Quadratic Configuration Interaction, Density Functional Theory, and Semiempirical Scale factors. J Phys Chem 100:16502–16513. https://doi.org/10.1021/jp960976r
42. Bhatia A, Chopra S, Nagpal K, Deb PK, Tekade M, Tekade RK (2018) Chapter 2 - polymorphism and its implications in Pharmaceutical Product Development. In: Tekade RK (ed) Dosage Form Design parameters. Academic, pp 31–65
43. Llinas A, Goodman JM (2008) Polymorph control: past, present and future. Drug Discov Today 13(5–6):198–210. https://doi.org/10.1016/j.drudis.2007.11.006
44. Wagner T, Schonleber A (2009) A non-mathematical introduction to the superspace description of modulated structures. Acta Crystallogr B 65(Pt 3):249–268. https://doi.org/10.1107/S0108768109015614
45. Ruck M (2000) Kristallographische Konsequenzen Von Pseudosymmetrie in Kristallstrukturen. Zeitschrift für Kristallographie -. Crystalline Mater 215(3):148–156. https://doi.org/10.1524/zkri.2000.215.3.148

46. Müller P (2006) Pseudo-symmetry. In: Müller P (ed) Crystal structure refinement: a crystallographer's guide to SHELXL. Oxford University Press, Oxford, United Kingdom, pp 97–105
47. Zwart PH, Grosse-Kunstleve RW, Lebedev AA, Murshudov GN, Adams PD (2008) Surprises and pitfalls arising from (pseudo) symmetry. Acta Crystallogr Sect D 64(1):99–107. https://doi.org/10.1107/S090744490705531X
48. Flack HD, Bernardinelli G (2000) Reporting and evaluating absolute-structure and absolute-configuration determinations. J Appl Crystallogr 33(4):1143–1148. https://doi.org/10.1107/S0021889800007184
49. Scilabra P, Terraneo G, Resnati G (2019) The Chalcogen Bond in Crystalline solids: a World parallel to Halogen Bond. Acc Chem Res 52(5):1313–1324. https://doi.org/10.1021/acs.accounts.9b00037
50. Vogel L, Wonner P, Huber SM (2019) Chalcogen Bonding: an overview. Angew Chem Int Ed 58(7):1880–1891. https://doi.org/10.1002/anie.201809432
51. Richter A, Patzer M, Goddard R, Lingnau JB, Imming P, Seidel RW (2022) Structural elucidation of the antitubercular benzothiazinone BTZ043: a combined X-ray, variable temperature NMR and DFT study. J Mol Struct 1248:131419. https://doi.org/10.1016/j.molstruc.2021.131419
52. Steed KM, Steed JW (2015) Packing problems: high Z' crystal structures and their relationship to cocrystals, inclusion compounds, and polymorphism. Chem Rev 115(8):2895–2933. https://doi.org/10.1021/cr500564z